Combined study of $\gamma p \to \eta p$ and $\pi^- p \to \eta n$ in a chiral constituent quark approach

Jun He*
Institute of Modern Physics, Chinese Academy of Sciences, Lanzhou 730000, People's Republic of China

B. Saghai†
Institut de Recherche sur les Lois Fondamentales de l'Univers, DSM/Irfu, CEA/Saclay, F-91191 Gif-sur-Yvette, France
(Received 9 December 2008; revised manuscript received 3 April 2009; published 24 July 2009)

Within a chiral constituent quark model approach, η-meson production on the proton via electromagnetic and hadron probes is studied. With few parameters, the differential cross section and polarized beam asymmetry for $\gamma p \to \eta p$ and differential cross section for $\pi^- p \to \eta n$ processes are calculated and successfully compared with the data in the center-of-mass energy range from threshold up to 2 GeV. The five known resonances $S_{11}(1535)$, $S_{11}(1650)$, $P_{13}(1720)$, $D_{13}(1520)$, and $F_{15}(1680)$ are found to be dominant in the reaction mechanisms in both channels. Possible roles played by new resonances are also investigated; and in the photoproduction channel, significant contribution from S_{11} and D_{15} resonances, with masses around 1715 and 2090 MeV, respectively, are deduced. For the so-called missing resonances, no evidence is found within the investigated reactions. The helicity amplitudes and decay widths of $N^* \to \pi N, \eta N$ are also presented and found to be consistent with the Particle Data Group values.

DOI: 10.1103/PhysRevC.80.015207 PACS number(s): 13.60.Le, 12.39.Fe, 12.39.Jh, 14.20.Gk

I. INTRODUCTION

Baryon spectroscopy is one of the major realms studied to deepen our understanding of QCD in the non-perturbative regime. Properties of the nucleon and its resonances are extracted mainly through photoproduction and/or hadron production of mesons off the nucleon.

In a recent paper [1], we investigated the $\gamma p \to \eta p$ process within a chiral constituent quark model and discussed the state-of-the art. In the present work, we extend that formalism to the $\pi^- p \to \eta n$ reaction and perform a combined analysis of both channels.

For the photoproduction process, a healthy amount of data has been released in recent years for both differential cross section [2–5] and polarized beam asymmetry [5,6]. The situation is very different for the $\pi^- p \to \eta n$ reaction. Actually, the data come mainly from measurements performed in the 1970s [7–12] and suffer from some inconsistencies [13]. A recent experiment, performed at BNL using the Crystal Ball spectrometer [14], offers a high quality data set, though limited to the close-to-threshold kinematics. Consequently, a combined database embodying experimental results for both electromagnetic and strong channels turns out to be highly heterogeneous. In spite of that uncomfortable situation, recent intensive theoretical investigations interpreting both channels within a single approach have proven to be fruitful in revealing various aspects of the relevant reaction mechanisms, as discussed, e.g., in Refs. [1,15].

In the photoproduction sector, significant progress has been made in recent years within coupled-channels formalisms [16–19] allowing the investigation of a large number of intermediate and/or final meson-baryon (MB) states: $\gamma N \to$ MB, with MB $\equiv \pi N, \eta N, \rho N, \sigma N, \pi\Delta, K\Lambda, K\Sigma$. Those approaches were reviewed in our recent paper [1]. Also advanced coupled-channels approaches are being developed [15,20–22] for the strong channels: $\pi N \to$ MB. However, fewer studies embody both electromagnetic and strong production processes. Moreover, those works are based on the effective Lagrangian approaches (ELA), where meson-baryon degrees of freedom are implemented (see, e.g., Refs. [17,18,23,24]). Investigations based on subnucleonic degrees of freedom via constituent quark models (CQM) have been successful [1,25–29] in the interpretation of photoproduction data on the proton, namely, $\gamma p \to \pi N, \eta p, K\Lambda$, and a recent work [30] has considered the $\pi^- p \to \eta n$ reaction.

At the present stage, the ELA and the CQM approaches are complementary. However, the QCD-inspired CQM developments deal on the one hand with more fundamental degrees of freedom and on the other hand require a much smaller number of adjustable parameters while fitting the data. This latter feature allows one to include a large number of resonances in the model search with still a reasonable number of free parameters. Hence, this approach turns out to be suitable in searching for the so-called missing and/or new resonances [18,26,28,31–40].

The present work is hence a step in a combined study of both electromagnetic and strong η-production processes within a unified chiral constituent quark (χQM) formalism.

The paper is organized as follows. In Sec. II, the theoretical content of our χQM approach is presented. The fitting procedure and numerical results for differential cross section, polarized beam asymmetry, helicity amplitudes, and partial decay widths are reported and discussed in Sec. III, where possible roles played by missing and new resonances are also examined. Summary and conclusion are given in Sec. IV.

II. THEORETICAL FRAME

To investigate hadrons and their resonances, various formalisms embodying the subnucleonic degrees of freedom are

*junhe@impcas.ac.cn
†bijan.saghai@cea.fr

being developed. Lattice QCD, based on the fundamental theory of strong interactions, is expected to establish the properties of hadrons, but there are still great technical difficulties when applied to resonances, see, e.g., Refs. [41,42]. The QCD sum rule approach is also applied to the resonance region, though limited to the low mass ones, such as $\Delta(1232)$ and $S_{11}(1535)$ [43–47]. That technique faces difficulties in controlling the uncertainties in handling phenomenological parameters. The most efficiently used approach to studying the baryon resonance is the constituent quark model, which provided the first clear evidence of the underlying SU(6) ⊗ O(3) structure of the baryon spectrum [48]. Subsequent studies have been concentrating mainly on the transition amplitudes and the baryon mass spectrum, achieving well-known successes [48–52], but they do not investigate reaction mechanisms.

To connect the constituent quark model to the reaction mechanisms of specific processes, a comprehensive and unified approach to the pseudoscalar meson photoproduction, based on the low-energy QCD Lagrangian [53], has been developed [54] and applied to some processes, including $\gamma p \to \eta p$ [25,26,55] and $\pi^- p \to \eta n$ [30,56].

In this section we recall briefly the content of the chiral constituent quark approach [1] and extend it to the η hadron-production process. As in Ref. [54], we start from an effective chiral Lagrangian [53],

$$\mathcal{L} = \bar{\psi}[\gamma_\mu(i\partial^\mu + V^\mu + \gamma_5 A^\mu) - m]\psi + \cdots, \tag{1}$$

where vector V^μ and axial A^μ currents read

$$V^\mu = \frac{1}{2}(\xi\partial^\mu\xi^\dagger + \xi^\dagger\partial^\mu\xi), \quad A^\mu = \frac{1}{2i}(\xi\partial^\mu\xi^\dagger - \xi^\dagger\partial^\mu\xi), \tag{2}$$

with $\xi = \exp(i\phi_m/f_m)$ and f_m the meson decay constant. ψ and ϕ_m are the quark and meson fields, respectively.

In this paper, we focus on the resonance contributions, for which the amplitudes can be written as

$$\mathcal{M}_{N^*} = \frac{2M_{N^*}}{s - M_{N^*}^2 - iM_{N^*}\Gamma(\mathbf{q})} e^{-\frac{\mathbf{k}^2+\mathbf{q}^2}{6\alpha^2}} \mathcal{O}_{N^*}, \tag{3}$$

where $\sqrt{s} \equiv W$ is the total energy of the system, and $\mathcal{O}_{N^*}$ is determined by the structure of each resonance. $\Gamma(\mathbf{q})$ in Eq. (3) is the total width of the resonance, and a function of the final state momentum $\mathbf{q}$.

The transition amplitude for the nth harmonic-oscillator shell is

$$\mathcal{O}_n = \mathcal{O}_n^2 + \mathcal{O}_n^3. \tag{4}$$

The first (second) term represents the process in which the incoming photon and outgoing meson are absorbed and emitted by the same (different) quark [30,54].

We use the standard multipole expansion of the CGLN amplitudes [57] to obtain the partial-wave amplitudes of resonance $f_{2I,2l\pm1}$. Then the transition amplitudes for pseudoscalar meson production through photon and meson baryon scattering take, respectively, the forms

$$\begin{aligned}\mathcal{O}_{N^*}^\gamma &= if_{1l\pm}\sigma\cdot\epsilon + f_{2l\pm}\sigma\cdot\hat{\mathbf{q}}\sigma\cdot(\hat{\mathbf{k}}\times\epsilon) \\ &\quad + if_{3l\pm}\sigma\cdot\hat{\mathbf{k}}\hat{\mathbf{q}}\cdot\epsilon + if_{4l\pm}\sigma\cdot\hat{\mathbf{q}}\epsilon\cdot\hat{\mathbf{q}}, \\ \mathcal{O}_{N^*}^m &= f_{1l\pm} + \sigma\cdot\hat{\mathbf{q}}\sigma\cdot\hat{\mathbf{k}}f_{2l\pm}.\end{aligned} \tag{5}$$

In Ref. [54], the partial decay amplitudes are used to separate the contribution of the state with the same orbital angular momentum L. As we found in Ref. [1], with the helicity amplitudes of photon transition and meson decay, we can directly obtain the CGLN amplitudes for each resonance in terms of Legendre polynomial derivatives. Analogously, the partial-wave amplitudes for pseudoscalar meson-baryon scattering are

$$\begin{aligned}f_1(\theta) &= \sum_{l=0}^{\infty}[f_{l+}P'_{l+1}(\cos\theta) - f_{l-}P'_{l-1}(\cos\theta)], \\ f_2(\theta) &= \sum_{l=0}^{\infty}[f_{l-} - f_{l+}]P'_l(\cos\theta),\end{aligned} \tag{6}$$

where θ is the angle of emission in the c.m. system.

We can connect the helicity amplitude for a certain resonance with the multipole coefficient, as in the case of the photoproduction process

$$\begin{aligned}f_{l\pm}^{N^*} &= \mp A_{l\pm}^{N^*} = \frac{1}{2}\epsilon\left(\frac{\Gamma_{m_i}\Gamma_{m_j}}{kq}\right)^{1/2} C_{m_iN}^{N^*}C_{m_jN}^{N^*} \\ &= \frac{1}{2\pi(2J+1)}\left(\frac{E_{N_i}E_{N_j}}{M_{N^*}^2}\right)^{1/2} A_{1/2}^{m_i}A_{1/2}^{m_j},\end{aligned} \tag{7}$$

where

$$\Gamma_m = \frac{1}{(2J+1)}\frac{|q|E_N}{\pi M_{N^*}}\left|A_{1/2}^m/C_{mN}^{N^*}\right|^2$$

is the decay width, and

$$C_{mN}^{N^*} = \langle I^{N^*}M^{N^*}|I^mM^mI^NM^N\rangle$$

are the Clebsch-Gordan coefficients, with m_i and m_j the incoming and outgoing mesons (respectively, π and η in this work).

In our approach, the photoexcitation helicity amplitudes A_λ^γ, as well as the strong decay amplitudes A_ν^m, are related to the matrix elements of the interaction Hamiltonian [48] as

$$A_\lambda = \sqrt{\frac{2\pi}{k}}\langle N^*; J\lambda|H_e\left|N; \frac{1}{2}\lambda - 1\right\rangle, \tag{8}$$

$$A_\nu^m = \left\langle N; \frac{1}{2}\nu\right| H_m|N^*; J\nu\rangle. \tag{9}$$

The amplitudes in Ref. [54] are derived under the SU(6) ⊗ O(3) symmetry. However, for physical states, that symmetry is broken. An example is the violation of the Moorhouse rule [58]. In Ref. [55], a set of parameters C_{N^*} were hence introduced to take into account the breaking of that symmetry, via the substitution

$$\mathcal{O}_{N^*} \to C_{N^*}\mathcal{O}_{N^*}. \tag{10}$$

In Refs. [26,55], those parameters were allowed to vary around their SU(6) ⊗ O(3) values ($|C_{N^*}| = 0$ or 1). In this work, instead of using those adjustable parameters, we introduce the breakdown of that symmetry through the configuration mixing of baryons wave functions, as we did in Ref. [1]. To achieve that improvement, we adopted the one-gluon-exchange (OGE) model [59–61], which has been successfully used to study the helicity amplitudes and decay widths of resonances [50].

III. RESULTS AND DISCUSSION

The most important and interesting nucleon resonances, such as $S_{11}(1535)$, are in the mass region lower than 2 GeV, that is, the $n = 1, 2$ shell states in the constituent quark model [59,62]. In this region, plentiful recent data are expected to give more reliable information about the internal structure and properties of baryon resonances. Hence, in the present work, we investigate the reactions $\gamma p \to \eta p$ and $\pi^- p \to \eta n$, focusing on the range of center-of-mass total energy from threshold up to $W \approx 2$ GeV, in order to interpret a large amount of high quality data released from various facilities.

A. Fitting procedure

Using the CERN MINUIT code, we fitted simultaneously the following data sets and the Particle Data Group (PDG) values:

(i) Spectrum of known resonances:

Known resonances: we use as input the PDG values [63] for masses and widths, with the uncertainties reported there plus an additional theoretical uncertainty of 15 MeV, as in Ref. [51], to avoid overemphasis of the resonances with small errors. The database contains all 12 known nucleon resonances as in PDG, with $M \leqslant 2$ GeV, namely,
$\mathbf{n = 1}$: $S_{11}(1535)$, $S_{11}(1650)$, $D_{13}(1520)$, $D_{13}(1700)$, and $D_{15}(1675)$;
$\mathbf{n = 2}$: $P_{11}(1440)$, $P_{11}(1710)$, $P_{13}(1720)$, $P_{13}(1900)$, $F_{15}(1680)$, $F_{15}(2000)$, and $F_{17}(1990)$.
Besides the above isospin-1/2 resonances, we fitted also the mass of the $\Delta(1232)$ resonance. However, spin-3/2 resonances do not intervene in η photoproduction. Concerning the resonances for which uncertainties are not given in PDG, we use 50 MeV.
Additional resonances: Resonances with masses above $M \approx 2$ GeV, treated as degenerate, are simulated by a single resonance, for which are left as adjustable parameters the mass, width, and symmetry-breaking coefficient.

(ii) Observables for $\gamma p \to \eta p$:

Differential cross section: Database includes 1220 data points for $1.49 \lesssim W \leqslant 1.99$ GeV, coming from the following laboratories: MAMI [64] (100 points), CLAS [2] (142 points), ELSA [3] (311 points), LNS [4] (180 points), and GRAAL [5] (487 points). Only statistical uncertainties are used.
Polarized beam asymmetry: 184 data points for $1.49 \lesssim W \leqslant 1.92$ GeV, from GRAAL [5] (150 points) and ELSA [6] (34 points). Only statistical uncertainties are used.
Target asymmetry: The target asymmetry (T) data [65] are not included in our database. Actually, those 50 data points bear too large uncertainties to put significant constraints on the parameters [25].

(iii) Observables for $\pi^- p \to \eta n$:

Differential cross section: Database includes 354 data points, for $1.49 \lesssim W \leqslant 1.99$ GeV, coming from Deinet [9] (80 points), Richards [11] (64 points), Debenham [12] (24 points), Brown [7] (102 points), and Prakhov [14] (84 points). Uncertainties are treated as in Ref. [15].

As already mentioned, for the $\pi^- p \to \eta n$ process, the data set is composed mainly of old data, plus those released recently by Prakhov *et al.* [14]. Models constructed [15,30,56] using those experimental results encountered some difficulties in reproducing especially the two lowest energy data sets. Those features deserve a few comments. The Prakhov *et al.* [14] data set consists of differential cross sections in nine incident pion momentum bins in the range $P_\pi = 687$ to 747 MeV/c, corresponding to the center-of-mass energy range $W = 1.49$ to 1.52 GeV. It is interesting to note that the reported total cross section increases by almost one order of magnitude going from the lowest to the highest pion momentum. To attenuate the undesirable effects of such sharp variations, we introduce an energy-dependent term in the denominator of the χ^2 expression used in the minimization procedure, namely,

$$\chi^2 = \sum \frac{(V_{\rm ex} - V_{\rm th})^2}{(\delta V_{\rm ex})^2 + (V'_{\rm th}\Delta E_{\rm ex})^2}. \tag{11}$$

Here $V_{\rm ex}$, $V_{\rm th}$, and $\delta V_{\rm ex}$ are the standard χ^2 quantities. The additional term is a product of the derivative of the observable with respect to energy ($V'_{\rm th}$), and the experimental energy bin ($\Delta E_{\rm ex}$). Notice that the data are reported for central values of $P_\pi \pm \Delta P_\pi$, with $\Delta P_\pi = 3$–7 MeV/c. We will come back to this point.

In summary, 1783 experimental values are fitted. To do so, we have a total of 21 free parameters, not all of them adjusted on all the data sets, as explained below.

In Table I, we report the list of adjustable parameters and their extracted values. Two of the parameters, namely, the nonstrange quark average mass m_q and the harmonic oscillator strength α are involved in fitting both mass spectrum and η-production data. The QCD coupling constant α_s and the confinement constants Ω and Δ intervene only in fitting the η-production data via the configuration mixing mechanism.

In Table I, the extracted values within the present work are compared with those reported in our previous paper. The only significant variation concerns the harmonic oscillator strength α, which is lowered by some 20%, as a result of including the strong channel. The quark mass is very close to the commonly used values, roughly one-third of the nucleon mass. For the other parameters, the extracted values here come out close to those used by Isgur and Karl [61] and Capstick and Roberts [52]: $E_0 = 1150$ MeV, $\Omega \approx 440$ MeV, and $\Delta \approx 440$ MeV. For the parameters α_s, α, and m_q, those researchers introduced $\delta = (4\alpha_s\alpha)/(3\sqrt{2\pi m_q^2})$, for which they obtained ≈300 MeV. Our model gives $\delta \approx 262$ MeV.

Among the remaining 16 adjustable parameters, nine of them (related to the new resonances) are extracted by fitting the photoproduction data, and the additional seven parameters are determined by fitting data for both channels. With respect to the η-nucleon coupling constant $g_{\eta NN}$, our result favors a rather small coupling around $g_{\eta NN} = 0.376$, which is compatible with those deduced from fitting only η photoproduction

TABLE I. Adjustable parameters with extracted values and χ^2, where m_q, α, Ω, Δ, M, and Γ are in MeV.

	Parameter	Model B in Ref. [1]	This work
	$g_{\eta NN}$	0.449	0.376
	m_q	304	312
	α	285	348
	α_s	1.98	1.96
	Ω	442	437
	Δ	460	460
HM N^*:	M	2129	2165
	Γ	80	80
	$C^{\gamma}_{N^*}$	−0.70	−0.84
	$C^{\pi}_{N^*}$	–	0.005
$P_{13}(1720)$:	$C^{\gamma}_{P_{13}(1720)}$	0.40	0.37
	$C^{\pi}_{P_{13}(1720)}$	–	−0.89
New S_{11}:	M^{γ}	1717	1715
	Γ^{γ}	217	207
	$C^{\gamma}_{N^*}$	0.59	0.51
New D_{13}:	M^{γ}	1943	1918
	Γ^{γ}	139	151
	$C^{\gamma}_{N^*}$	−0.19	−0.19
New D_{15}:	M^{γ}	2090	2090
	Γ^{γ}	328	345
	$C^{\gamma}_{N^*}$	2.89	2.85
$\sum \chi^2_{dp}/N_{dp}$:	χ^2 for total	$3273/1418 = 2.31$	$3627/1772 = 2.05$
	χ^2_{γ} for $\gamma p \to \eta p$	$3243/1404 = 2.31$	$3187/1404 = 2.27$
	χ^2_{π} for $\pi^- p \to \eta n$	–	$408/354 = 1.15$
	Spectrum	$30/14 = 2.14$	$32/14 = 2.29$

[26,55]. Comparable values for the coupling are also reported in Refs. [66–69].

The parameter $C_{P_{13}(1720)}$ is the strength of the $P_{13}(1720)$ resonance, which we had to leave as a free parameter to avoid its too large contribution resulting from direct calculation, as discussed in Ref. [1]. The value of that parameter for the photoproduction reaction is close to that in our previous paper. For the strong channel, $C^{\pi}_{P_{13}(1720)}$ turns out to be larger in magnitude than that of photoproduction, $C^{\gamma}_{P_{13}(1720)}$.

The higher mass resonance (HM N^*) treatment requires four adjustable parameters: M, Γ, $C^{\gamma}_{N^*}$, and $C^{\pi}_{N^*}$, which are determined by fitting the η-production data. Here, different strengths ($C^{\gamma}_{N^*}$ and $C^{\pi}_{N^*}$) for higher mass resonances and $P_{13}(1720)$ are used, because two processes have different initial states. Notice that in fitting the η-production data, we use the PDG [63] values for masses and widths of the known resonances.

In recent years, several authors [18,26,28,31–40] have put forward a need for new resonances in interpreting various observables, with extracted masses roughly between 1.7 and 2.1 GeV. We have hence investigated possible contributions from three of them: S_{11}, D_{13}, and D_{15}. For each of those new resonances, we then introduced three additional adjustable parameters per resonance: mass M, width Γ, and symmetry-breaking coefficient C_{N^*}. For the three new resonances, we follow the method in Ref. [55] via Eq. (10). The computed Wigner masses and widths, as well as the strengths for those resonances, are given in Table I. The results are close to those in Ref. [1].

For the process $\pi^- p \to \eta n$, given the state of the database, the determination of the reaction mechanism is less reliable than for photoproduction. Consequently, a search for signals from unknown resonances in that strong channel would be superfluous. Nevertheless, we looked at possible contributions from those three new resonances and found their contributions negligible. Accordingly, for the strong channel, we deal only with the known resonances.

As shown in Table I, the χ^2 for both processes is 2.05, with 2.27 for the η photoproduction and 1.15 for $\pi^- p \to \eta n$. So, within our model, the data are well enough reproduced. With respect to the latter channel, if we do not consider the uncertainty for the energy [Eq. (11)] and use the same definition for χ^2 as the EBAC Collaboration [15], we obtain $\chi^2 = 1.99$ for $\pi^- p \to \eta n$, which is close to its EBAC value, 1.94.

To end this section, we examine the role played by each of the 12 known, three new, and one heavy mass resonances. To that end, we have switched off resonances one by one. The results are reported in Table II. For each case, two numbers are given corresponding to two sets of χ^2: (i) without further minimization and (ii) after minimization (in brackets). That table embodies results for seven resonances. For the remaining

TABLE II. χ^2 after turning off the corresponding resonance contribution, without [with] further minimizations, including partial χ^2 for the $\gamma p \to \eta p$ and $\pi^- p \to \eta n$ processes.

	$S_{11}(1535)$	$S_{11}(1650)$	$P_{13}(1720)$	$D_{13}(1520)$	$F_{15}(1680)$	New S_{11}	New D_{15}
χ^2	136 [80]	12.3 [2.36]	3.49 [2.90]	9.60 [5.27]	4.33 [3.25]	9.63 [4.44]	3.37 [2.34]
χ^2_γ	160 [85]	14.2 [2.60]	3.55 [2.77]	10.04 [5.79]	4.44 [3.59]	11.84 [5.22]	3.93 [2.60]
χ^2_π	48 [65]	4.9 [1.40]	3.31 [3.38]	8.17 [3.32]	3.98 [1.91]	1.16 [1.39]	1.16 [1.28]

nine resonances, the variations of χ^2 were found negligible and hence are not shown in the table. However, in some regions in the phase space, a few of those resonances play significant roles, and we will emphasize those features in the relevant sections.

For the known resonances in PDG, as expected, the most important role is played by the $S_{11}(1535)$. The effects of $S_{11}(1650)$ and $D_{13}(1520)$, and to a lesser extent those of $F_{15}(1680)$ and $P_{13}(1720)$, turn out to be very significant. In addition to those known resonances, a new S_{11} appears to be strongly needed by the photoproduction data. We also investigated possible contributions from the missing resonances (see next section) following the above procedure and found no significant effects.

In the following, we will first present our results for the baryon spectrum. Then we will move to the observables for the $\gamma p \to \eta p$ and $\pi^- p \to \eta n$ processes and compare our model with the data. To give better insight into the reaction mechanism, we will also report on our results obtained by turning off the resonances that have significant effects on χ^2 for both processes studied here without further minimizations.

B. Baryon spectrum

The baryon spectrum results computed from the present work are reported in Table III. They are in good agreement with those obtained by Isgur and Karl [60,61], and except for the $S_{11}(1535)$ and $D_{13}(1520)$ resonance results, they fall in the ranges estimated by PDG [63]. The additional missing resonances generated by the OGE model are also shown in Table III. The computed masses are compatible with those reported by Isgur and Karl [60,61].

C. Observables for $\gamma p \to \eta p$

This section is devoted to the results for differential cross sections $d\sigma/d\Omega$ and polarized beam asymmetries Σ for $\gamma p \to \eta p$, as in our previous work [1], as well as those for the total cross section.

First, to give an overall picture of various features of our model, we present the results for the total cross section and compare them with the data (Fig. 1). Notice that the data for the total cross section are not used in minimization.

Our full model gives a reasonable account of the total cross section behavior from threshold up to 2 GeV with a small discrepancy around $W = 1.9$ GeV. In Fig. 1, we also show results obtained by turning off the most significant resonances, without further minimizations.

Switching off the $S_{11}(1535)$ resonance decreases the close-threshold cross section by more than two orders of magnitude. At energies far above threshold, the absence of that resonance shows still non-negligible effects. The contribution of the second S_{11} resonance, $S_{11}(1650)$, is visible from about 1.55 GeV up to 1.75 GeV. As reported in Table II, turning off that resonance increases the χ^2 from 2.05 to 12.3 without further minimization and to 2.36 after minimization. The significant discrepancy between the two χ^2 can be understood by the fact that in the same mass region, there are two other relevant resonances [new S_{11} and $P_{13}(1720)$], and by redoing minimizations their relative strengths get new values. Such a "compensating" mechanism shows up also in effective Lagrangian-based models through the extracted $\eta N N^*$

TABLE III. Computed masses (in MeV) for the known PDG and so-called missing resonances compared with the values by Isgur *et al.* [60,61] and PDG [63].

PDG resonances	$S_{11}(1535)$	$S_{11}(1650)$	$P_{11}(1440)$	$P_{11}(1710)$	$P_{13}(1720)$	$P_{13}(1900)$
$M^{\rm OGE}$, this work	1471	1617	1423	1720	1712	1847
$M^{\rm OGE}$ [60,61]	1490	1655	1405	1705	1710	1870
$M^{\rm PDG}$ [63]	1535 ± 10	1655^{+15}_{-10}	1440^{+30}_{-20}	1710 ± 30	1720^{+30}_{-20}	1900
PDG resonances	$D_{13}(1520)$	$D_{13}(1700)$	$D_{15}(1675)$	$F_{15}(1680)$	$F_{15}(2000)$	$F_{17}(1990)$
$M^{\rm OGE}$, this work	1509	1697	1629	1717	2002	1939
$M^{\rm OGE}$ [60,61]	1535	1745	1670	1715	2025	1955
$M^{\rm PDG}$ [63]	1520 ± 5	1700 ± 50	1675 ± 5	1685 ± 5	2000	1990
Missing resonances	P_{11}	P_{11}	P_{13}	P_{13}	P_{13}	F_{15}
$M^{\rm OGE}$, this work	1893	2044	1936	1959	2041	1937
$M^{\rm OGE}$ [61]	1890	2055	1955	1980	2060	1955

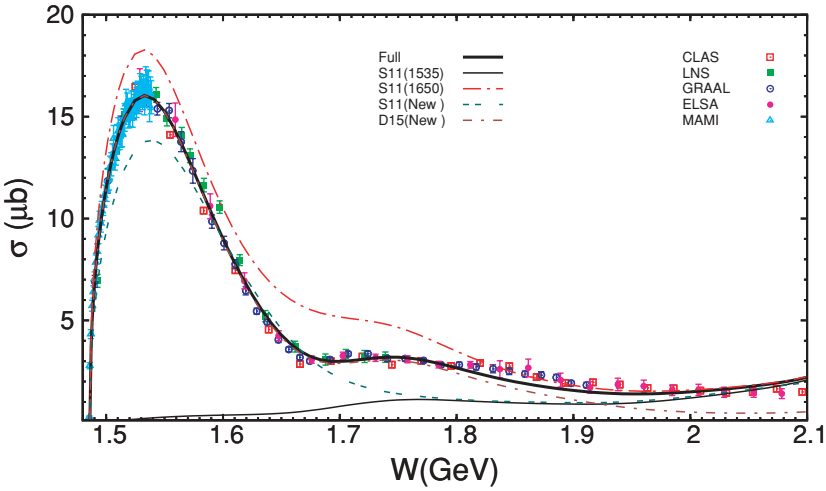

FIG. 1. (Color online) Total cross section for $\gamma p \to \eta p$ as a function of total center-of-mass energy W. The curves and data points are identified in the legend. Data are from CLAS [2], LNS [4], GRAAL [5], ELSA [3], and MAMI [64].

couplings. The new S_{11} resonance turns out playing a significant role roughly between 1.7 and 1.8 GeV. Finally, a new D_{15} appears, affecting the highest energy region investigated here.

Excitation functions for differential cross sections and polarized beam asymmetries are presented in Fig. 2, left and right panels, respectively. For differential cross sections, model vs data comparisons lead to similar conclusions as in the case of total cross sections, with respect to the model ingredients. Moreover, the underestimation of data around 1.85–1.95 GeV turns out to happen at forward angles.

Results for the polarized beam asymmetries are shown in the right panel in Fig. 2. Here also the $S_{11}(1535)$ is

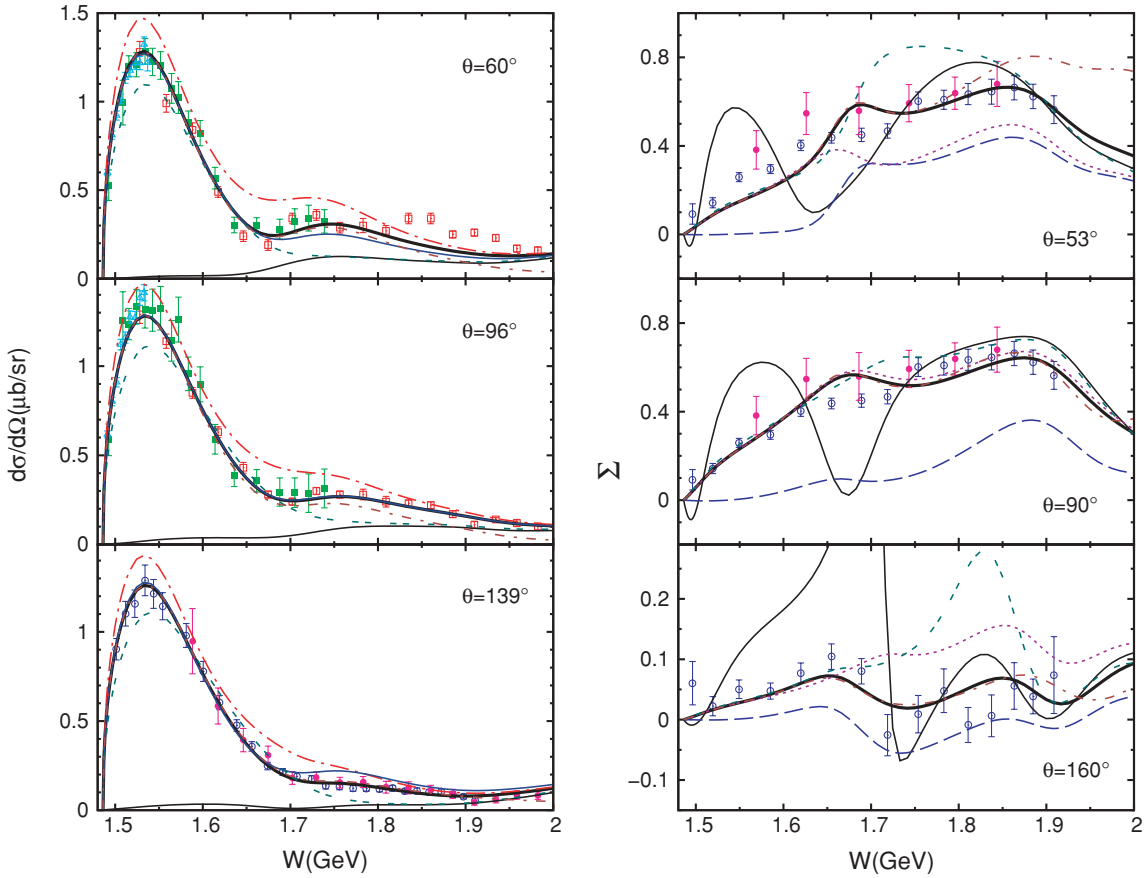

FIG. 2. (Color online) Differential cross section (left panel) and polarized beam asymmetry (right panel) for $\gamma p \to \eta p$ as a function of W at three angles. Both panels show curves for the full model (thick full) and turning off $S_{11}(1535)$ (thin full), new S_{11} (dash-dashed), and new D_{15} (short dash-dotted). The left panel shows the curves for switching off $S_{11}(1650)$ (long dash-dotted) and $P_{13}(1720)$ (dashed); right panel shows those for turning off $D_{13}(1520)$ (dashed) and $F_{15}(1680)$ (dotted). Data are as in Fig. 1.

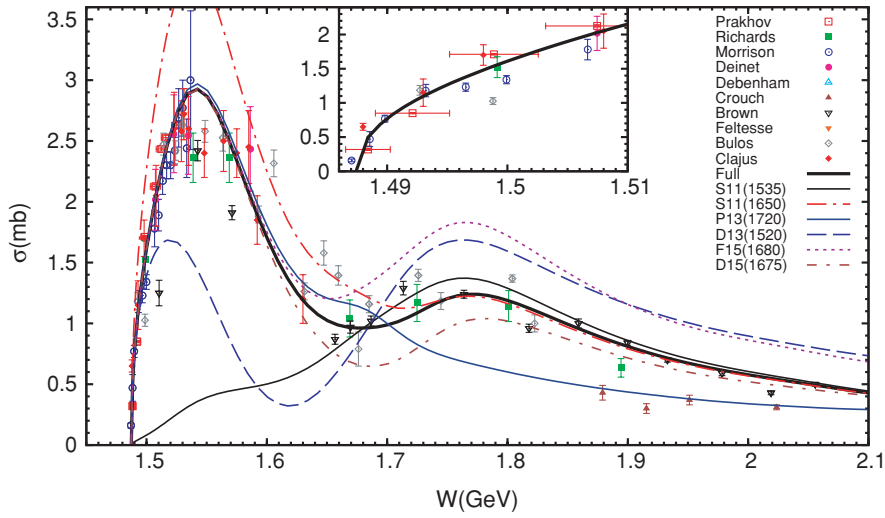

FIG. 3. (Color online) Total cross section for $\pi^- p \to \eta n$ as a function of W. The curves are for the full model and for turning off individual resonances (see legend). Data are from Prakhov [14], Richards [11], Morrison [70], Deinet [9], Debenham [12], Crouch [71], Brown [7], Feltesse [10], Bulos [8,72], and Clajus [13]. The inserted box shows the near-threshold energy range.

still the most dominant ingredient up to roughly 1.75 GeV. In contrast to the cross section reaction mechanism, we observe significant contributions from two known resonances. Actually, the $D_{13}(1520)$ plays the second important role. Its effect is most spectacular around 90°. On the contrary, the $F_{15}(1680)$ has important contributions far from 90°.

Finally, two new resonances seem to be needed to reproduce the data. The new S_{11} resonance shows up especially at backward angles and to a lesser extent at forward angles, with the spanned energy range located between 1.7 and 1.85 GeV. Contributions from the new D_{15} resonance are limited to forward angles and high energies.

This section, devoted to the observables of the process $\gamma p \to \eta p$ in the energy range $W \lesssim 2$ GeV, leads to the conclusion that within our approach, the reaction mechanism is dominant by five known and two new nucleon resonances; that is, $S_{11}(1535)$, new S_{11}, and to a lesser extent D_{15} intervene significantly in both observables, while $S_{11}(1650)$ and $P_{13}(1720)$ have impact on the cross section, and $D_{13}(1520)$ and $F_{15}(1680)$ play important roles in polarized beam asymmetry.

D. Observables for $\pi^- p \to \eta n$

We start with presenting the total cross section (Fig. 3). As in the photoproduction case, $S_{11}(1535)$ makes the most dominant contribution. The contribution of the second S_{11} resonance, $S_{11}(1650)$, turns out to be important, though in a restricted part of the phase space. Its vanishing contribution close to 1.7 GeV is compensated by the appearance of contributions from $F_{15}(1680)$. The first S_{11} has a constructive contribution, while that of the second one and $F_{15}(1680)$ are destructive. $D_{13}(1520)$ plays the second most important role. The peculiar effect of this resonance could be attributed to strong interferences with other partial waves; it starts as constructive before turning, around 1.7 GeV, to destructive behavior. As found in Refs. [25,30], the second peak is from the contribution of $n = 2$ shell resonances, and the result in this work endorses that the $P_{13}(1720)$ accounts for that peak. Finally, contributions from $D_{15}(1675)$ show up around 1.7 GeV.

Here, we would like to return to the recent data released by Prakhov *et al.* [14] in relation to our discussion in Sec. III A and Eq. (11). In the box at the top of Fig. 3, we have expanded the energy region $W \leqslant 1.51$ GeV. The spread of the energy bin [$\Delta E_{\rm ex}$ in Eq. (11)] compared with the cross section uncertainties and the fact that the cross section rises very rapidly with energy explain the difficulties in fitting the lowest energy data (Fig. 3). In that box, it can be seen that our full model crosses the energy bands but not always the experimental values for the cross section. Actually, using the standard definition of χ^2, those data points give very large contributions and render the fitting procedure somewhat problematic. That undesirable behavior can be attenuated by embodying the energy bin in the χ^2 determination, as in Eq. (11).

Now, we move to differential cross sections, depicted in Figs. 4 and 5, and examine the reaction mechanism ingredients.

The full model reproduces the data reasonably well, with less success in the close-threshold region, as discussed above. The highly dominant role of $S_{11}(1535)$ is present in the whole energy range investigated here, from threshold up to about 1.6 GeV (Fig. 4). Above that energy, as seen in the total cross section plot, the effect of that resonance rapidly vanishes with energy. In the low-energy region, $W \lesssim 1.6$ GeV, we show also results with $S_{11}(1650)$ or $D_{13}(1520)$ turned off. In both cases, the effects are significant, and the latter resonance generates the correct curvature required by the data.

Figure 5 shows results for the higher energy region, where the data are less consistent with each other than in the lower energy region. Obviously the data by Crouch *et al.* [71] cannot be simultaneously fitted with those by Brown *et al.* [7]. Here, following Ref. [15], we choose the latter in the fitting procedure. In going from the low-energy to the high-energy region the shape of the theoretical results changes: a structure at forward angles appears, while the slope in the backward hemisphere becomes more and more attenuated with energy increase.

The full model reproduces well enough this heterogeneous database. By switching off the resonances one by one, we show in that figure that the most significant effects are due to $P_{13}(1720)$, $D_{13}(1520)$, $F_{15}(1680)$, and $D_{15}(1675)$, which appear mainly at forward hemisphere and to a lesser extent in the most backward angles. $D_{13}(1520)$ produces the correct curvature at the most forward angles. Roughly in the same

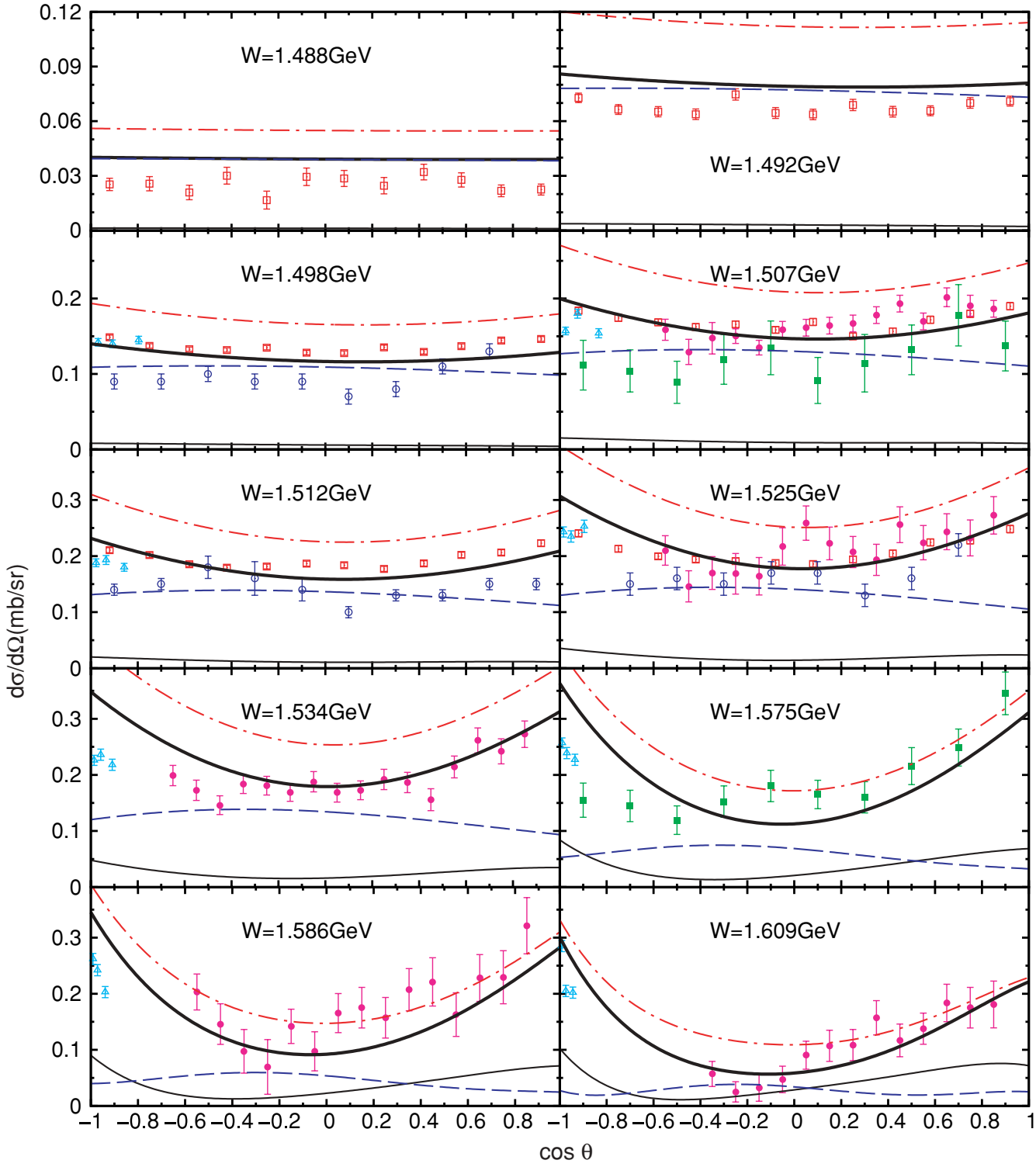

FIG. 4. (Color online) Differential cross section for $\pi^- p \to \eta n$ as a function of $\cos\theta$ at lower energies. The curves are for the full model (thick full) and for turning off $S_{11}(1535)$ (thin full), $S_{11}(1650)$ (dash-dotted), and $D_{13}(1520)$ (dashed) resonances. Data as in Fig. 3.

angular region, the $F_{15}(1680)$ resonance plays a significant role. Both of those resonances show destructive contributions. Constructive effects are caused by $P_{13}(1720)$ and $D_{15}(1675)$, with comparable strengths in the whole forward angle region.

This section, focused on the observables of the process $\pi^- p \to \eta n$ in the energy range $W \lesssim 2$ GeV, leads to the conclusion that within our approach, the reaction mechanism is dominated by six known resonances: $S_{11}(1535)$, $S_{11}(1650)$, $P_{13}(1720)$, $D_{13}(1520)$, $D_{15}(1675)$, and $F_{15}(1680)$.

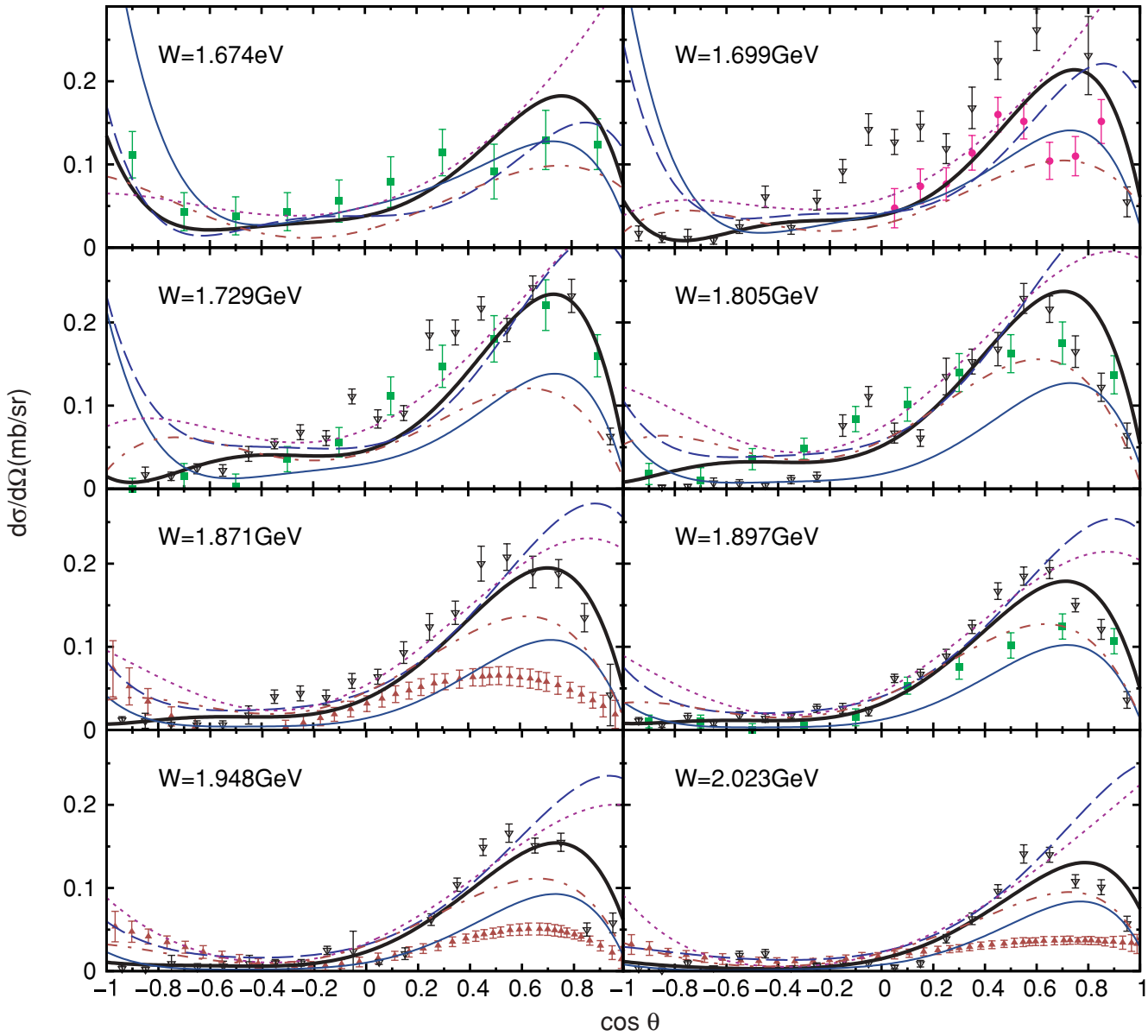

FIG. 5. (Color online) Same as Fig. 4, but at higher energies. The curves are for the full model (thick full) and for turning off $P_{13}(1720)$ (dashed), $D_{15}(1675)$ (short dash-dotted), $D_{13}(1520)$ (long dashed), and $F_{15}(1680)$ (thin dashed).

E. Helicity amplitudes and partial decay widths

After fitting the observables, we can calculate the helicity amplitudes and the partial decay widths for $N^* \to \eta N$ or πN within a given model without adjustable parameters. Results corresponding to our full model are presented in Table IV for all $n = 1$ and 2 shell resonances generated by the quark model including the so-called missing ones.

The helicity amplitudes are in line with results from other similar approaches (see Tables I and II in Ref. [52]). Except for $S_{11}(1535)$, the decay widths for πN are much larger than those for the ηN case.

For the dominant known resonances, $S_{11}(1535)$ and $S_{11}(1650)$, the helicity amplitudes and decay widths for both decay channels are in good agreement with the PDG values. That is also the case for the $A_{3/2}$ values and decay widths of both $D_{13}(1520)$ and $F_{15}(1680)$. For the latter resonance, $A_{1/2}$ has the right magnitude but opposite sign with respect to the PDG value. However, for that resonance, with $A_{3/2}$ being much larger than $A_{1/2}$, the effect of the latter amplitude is not significant enough in computing the observables. The helicity amplitudes as well as the πN decay width for $P_{13}(1720)$ deviate significantly from their PDG values, as is also the case in other relevant approaches (see Table II in Ref. [52]). Those large values produced by our model forced us to treat the symmetry-breaking coefficient for $P_{13}(1720)$ as a free parameter (Table I) in order to suppress its otherwise too large contribution. As far as the other known resonances are concerned, we get results compatible with the PDG values for $D_{13}(1700)$ and $F_{17}(1990)$, and to a lesser extent for $D_{15}(1675)$. Finally, we put forward predictions for the missing resonances,

TABLE IV. Helicity amplitudes and decay widths for resonances, with $\Gamma^{\rm PDG}_{\eta(\pi)N} = \Gamma_{\rm tot} \times {\rm Br}_{\eta(\pi)N}$ in PDG [63]. Here σ is the sign for $\pi N \to \eta N$ as in Ref. [50].

Resonance	$A_{1/2}$	$A^{\rm PDG}_{1/2}$	$A_{3/2}$	$A^{\rm PDG}_{3/2}$	$\sigma\sqrt{\Gamma_{\eta N}}$	$(\sigma)\sqrt{\Gamma^{\rm PDG}_{\eta N}}$	$\sqrt{\Gamma_{\pi N}}$	$\sqrt{\Gamma^{\rm PDG}_{\pi N}}$
$S_{11}(1535)$	73	90 ± 30			7.18	$8.87^{+1.37}_{-1.37}$	6.78	$8.22^{+1.59}_{-1.60}$
$S_{11}(1650)$	66	53 ± 16			−2.42	$1.95^{+0.94}_{-1.57}$	8.85	$11.31^{+1.95}_{-1.98}$
$P_{11}(1440)$	−23	-65 ± 4			−2.42		17.16	$13.96^{+4.41}_{3.48}$
$P_{11}(1710)$	−53	9 ± 22			−1.05	$2.49^{+1.75}_{-0.88}$	4.12	$3.87^{+3.20}_{-1.64}$
P_{11}	18				−2.79		6.59	
P_{11}	3				−1.20		4.51	$5.34^{+2.16}_{-2.16}$
$P_{13}(1720)$	177	18 ± 30	−69	-19 ± 20	2.91	$2.83^{+1.04}_{-0.71}$	20.15	$5.48^{+2.27}_{-1.60}$
$P_{13}(1900)$	30		2		−1.33	$8.35^{+2.11}_{-2.20}$	11.02	$11.38^{+2.20}_{-2.21}$
P_{13}	28		0		2.44		3.06	
P_{13}	12		2		0.03		5.54	
P_{13}	−3		3		−1.01		3.12	
$D_{13}(1520)$	−7	-24 ± 9	158	166 ± 5	0.44	$0.51^{+0.07}_{-0.06}$	14.77	$8.31^{+0.71}_{-0.53}$
$D_{13}(1700)$	−4	-18 ± 13	4	-2 ± 24	−0.81	$0.00^{+1.22}_{-0.00}$	4.92	$3.16^{+1.58}_{-1.58}$
$D_{15}(1675)$	−6	19 ± 8	−8	15 ± 9	−2.50	$0.00^{+1.28}_{-0.00}$	7.59	$7.75^{+0.87}_{-1.00}$
$F_{15}(1680)$	24	-15 ± 6	136	133 ± 12	0.58	$0.00^{+1.18}_{-0.00}$	13.71	$9.37^{+0.53}_{-0.54}$
F_{15}	−9		4		0.97		0.35	
$F_{15}(2000)$	−1		10		−0.47		3.60	$4.00^{+6.20}_{-2.18}$
$F_{17}(1990)$	5	1	6	4	−1.55	$0.00^{+2.17}_{-0.00}$	6.84	$4.58^{+1.55}_{-1.55}$

for which we find rather small amplitudes, explaining the negligible roles played by them in our model.

IV. SUMMARY AND CONCLUSION

In the present work, we have presented a unified description of the processes $\gamma p \to \eta p$ and $\pi^- p \to \eta n$ within a chiral constituent quark approach, extending our previous investigation of the photoproduction channel to the $\pi^- p$ initial state. Our approach embodies the breaking of the SU(6) $\otimes$ O(3) symmetry, via a one-gluon-exchange mechanism. The generated configuration mixing is characterized by mixing angles, which we have determined without specific free parameters. Moreover, the present quark approach is used to derive photoexcitation helicity amplitudes and partial decay widths of the nucleon resonances to πN and ηN final states.

Our study is focused on the reaction mechanisms of the considered reactions in the energy range from threshold up to the center-of-mass energy $W \approx 2$ GeV, where data for both reactions are available. Accordingly, the nucleon resonances taken into account are explicitly dealt with for $n \leqslant 2$ harmonic oscillator shells. Within that framework, we have successfully fitted close to 1800 data points with 21 adjustable parameters, with nine of them related to the three new resonances. With such a rather small number of free parameters, we have investigated possible roles played in those reaction mechanisms by 12 known resonances, six the so-called missing resonances, and three new ones.

The combined fit of the known baryon spectrum and the $\gamma p \to \eta p$ measured observables allowed us to (i) extract the masses of missing resonances generated by the used formalism, (ii) extract the mixing angles between relevant configurations, which came out [1] in agreement with Isgur-Karl pioneer work, and (iii) determine the parameters of the three new resonances, compatible with other findings.

The reaction mechanism for the process $\gamma p \to \eta p$ is found, as expected, to be dominated by the $S_{11}(1535)$ resonance, with significant contributions from four additional known resonances [$S_{11}(1650)$, $D_{13}(1520)$, $F_{15}(1680)$, and $P_{13}(1720)$], and from a new resonance, $S_{11}(1717)$. The importance of those five known resonances is corroborated by the calculated photoexcitation helicity amplitudes and final-state ηp branching ratios.

For the photoproduction channel, the new S_{11} resonance turns out to be essential in reproducing the data, for which the extracted Wigner mass and width come out consistent with the values in Refs. [26,28,31,32], but the mass is lower, by about 100–200 MeV, than findings by other authors [34–37,73]. The most natural explanation would be that it is the first S_{11} state in the $n = 3$ shell. However, its low mass could indicate a multiquark component, such as a quasibound kaon-hyperon [32] or pentaquark configuration [74]. In Ref. [75], the authors propose an $N^*(1685)$ resonance from the reanalysis of the GRAAL beam asymmetry data, but their results do not support an S partial-wave resonance.

Cutkosky *et al.* [76] reported a D_{13} resonance at 1880 $\pm$ 100 MeV with 180 $\pm$ 60 MeV widths. Recent investigations found a $D_{13}(1875)$ state coupling strongly to the kaon-hyperon channels but not to the ηN channel [24,77]. In this work, we also find that for the new D_{13} resonance, the variation of χ^2 is smaller than that for other resonances. Interestingly, we find a large effect from a D_{15} state around 2090 GeV with a

Wigner width of 330 MeV. It is very similar to the $N(2070)D_{15}$ reported in Refs. [3,18,24]. It can be explained as the first D_{15} state in the $n = 3$ shell [3].

We come back to the known P- and D-wave resonances, in the mass energy region around 1.71 GeV, and hence the most important energy region to study the $n = 2$ shell resonances, in both processes investigated here. The literature has reported different conclusions on the relative weight of the relevant resonances in the reaction mechanism. In Ref. [78], the inclusion of the $P_{13}(1720)$ resonance does not improve significantly the description of the data for the photoproduction, while this resonance considerably improves the fit quality of the hadronic $\pi^- p \to \eta n$ reaction at higher energies, and the small bump near $W = 1.7$ GeV in the spin-1/2 resonance contribution is attributed to the $P_{11}(1710)$ resonance. In Ref. [79], this latter resonance together with the background contributions dominates the $\pi^- p \to \eta n$ reaction in the $n = 2$ shell energy area, developing a peak in the total cross section around 1.7 GeV. As in Ref. [80], our results endorse the $n = 2$ shell resonances $P_{13}(1720)$, not the $P_{11}(1710)$, providing the most significant contribution in both η production processes. A recent quark model approach [30] found important effects due to the $P_{11}(1720)$ in the $\pi^- p \to \eta n$, but it did not consider the SU(6) $\otimes$ O(3) symmetry breaking. In the present work, the crucial character of this latter mechanism attenuates the role attributed to $P_{11}(1720)$. However, our results do not allow us to reach firm conclusions about the role of the P-wave resonances. The origin of this situation can be traced back to the discrepancies between the calculated photoexcitation amplitudes for the $P_{13}(1720)$ and those reported in PDG. Such discrepancies are also found in other constituent quark model calculations [52]. This may indicate that the $P_{13}(1720)$ has a more complicated structure than the simple three-quark picture. In Ref. [80], the $D_{13}(1700)$ resonance gives the largest contribution to the cross section in the energy region of $W = 1.7$–2.0 GeV, but we do not find such contributions from the $D_{13}(1700)$.

To summarize our findings with respect to the $\pi^- p \to \eta n$, we emphasize that within our approach, besides those from the (by far) dominant $S_{11}(1535)$, significant contributions are also found from the same four known resonances [$S_{11}(1650)$, $D_{13}(1520)$, $F_{15}(1680)$, and $P_{13}(1720)$] as in the photoproduction case. For the strong channel, another resonance turns out to relevant, namely, $D_{15}(1675)$.

From a theoretical point of view, the next steps are to (i) perform a comprehensive extended coupled-channels study [81], (ii) extend the present formalism to higher n shells to investigate all photoproduction data up to $W \approx 2.6$ GeV, embodying all PDG one to four star resonances [82]. In the experimental sector, the most needed data concern the $\pi^- p \to \eta n$ channel. Double polarization observables for $\gamma p \to \eta p$ planned to be measured at the Thomas Jefferson National Accelerator Facility [83] will certainly improve our understanding of the underlying reaction mechanisms.

ACKNOWLEDGMENTS

We are grateful to Johan Durand for providing the database for $\pi^- p \to \eta n$.

[1] J. He, B. Saghai, and Z. Li, Phys. Rev. C **78**, 035204 (2008).
[2] M. B. Dugger *et al.* (CLAS Collaboration), Phys. Rev. Lett. **89**, 222002 (2002).
[3] V. Crede *et al.* (CB-ELSA Collaboration), Phys. Rev. Lett. **94**, 012004 (2005).
[4] T. Nakabayashi *et al.*, Phys. Rev. C **74**, 035202 (2006).
[5] O. Bartalini *et al.* (GRAAL Collaboration), Eur. Phys. J. A **33**, 169 (2007).
[6] D. Elsner *et al.* (CB-ELSA Collaboration), Eur. Phys. J. A **33**, 147 (2007).
[7] R. M. Brown *et al.*, Nucl. Phys. **B153**, 89 (1979).
[8] F. Bulos *et al.*, Phys. Rev. **187**, 1827 (1969).
[9] W. Deinet *et al.*, Nucl. Phys. **B11**, 495 (1969).
[10] J. Feltesse *et al.*, Nucl. Phys. **B93**, 242 (1975).
[11] W. B. Richards *et al.*, Phys. Rev. D **1**, 10 (1970).
[12] N. C. Debenham *et al.*, Phys. Rev. D **12**, 2545 (1975).
[13] M. Clajus and B. M. K. Nefkens, PiN Newslett. **7**, 76 (1992).
[14] S. Prakhov *et al.*, Phys. Rev. C **72**, 015203 (2005).
[15] J. Durand, B. Julia-Diaz, T. S. H. Lee, B. Saghai, and T. Sato, Phys. Rev. C **78**, 025204 (2008).
[16] W.-T. Chiang, S. N. Yang, L. Tiator, M. Vanderhaeghen, and D. Drechsel, Phys. Rev. C **68**, 045202 (2003).
[17] T. Feuster and U. Mosel, Phys. Rev. C **59**, 460 (1999).
[18] A. V. Sarantsev *et al.*, Eur. Phys. J. A **25**, 441 (2005).
[19] R. A. Arndt, W. J. Briscoe, I. I. Strakovsky, and R. L. Workman, Int. J. Mod. Phys. A **22**, 349 (2007).
[20] Wen-Tai Chiang, B. Saghai, F. Tabakin, and T. S. H. Lee, Phys. Rev. C **69**, 065208 (2004).
[21] B. Julia-Diaz, T. S. H. Lee, A. Matsuyama, and T. Sato, Phys. Rev. C **76**, 065201 (2007).
[22] J. Durand, B. Julia-Diaz, T. S. H. Lee, B. Saghai, and T. Sato, Int. J. Mod. Phys. A **24**, 553 (2009).
[23] G. Penner and U. Mosel, Phys. Rev. C **66**, 055212 (2002).
[24] A. V. Anisovich *et al.*, Eur. Phys. J. A **25**, 427 (2005).
[25] J. He, B. Saghai, Z. Li, Q. Zhao, and J. Durand, Eur. Phys. J. A **35**, 321 (2008).
[26] B. Saghai and Z. Li, Eur. Phys. J. A **11**, 217 (2001).
[27] Qiang Zhao, J. S. Al-Khalili, Z. P. Li, and R. L. Workman, Phys. Rev. C **65**, 065204 (2002).
[28] B. Julia-Diaz, B. Saghai, T.-S. H. Lee, and F. Tabakin, Phys. Rev. C **73**, 055204 (2006).
[29] B. Saghai, J.-C. David, B. Julia-Diaz, and T. S. H. Lee, Eur. Phys. J. A **31**, 512 (2007).
[30] X.-H. Zhong, Q. Zhao, J. He, and B. Saghai, Phys. Rev. C **76**, 065205 (2007).
[31] M. Batinic, I. Dadic, I. Slaus, A. Svarc, and B. M. K. Nefken, arXiv:nucl-th/9703023.
[32] Z. Li and R. Workman, Phys. Rev. C **53**, R549 (1996).
[33] N. G. Kelkar and B. K. Jain, Nucl. Phys. **A612**, 457 (1997).
[34] M. M. Giannini, E. Santopinto, and A. Vassallo, Eur. Phys. J. A **12**, 447 (2001).
[35] G.-Y. Chen, S. Kamalov, S. N. Yang, D. Drechsel, and L. Tiator, Nucl. Phys. **A723**, 447 (2003).

[36] W. T. Chiang, S. N. Yang, M. Vanderhaeghen, and D. Drechsel, Nucl. Phys. **A723**, 205 (2003).
[37] V. A. Tryasuchev, Eur. Phys. J. A **22**, 97 (2004).
[38] T. Mart, A. Sulaksono, and C. Bennhold, arXiv:nucl-th/0411035.
[39] M. Ablikim *et al.* (BES Collaboration), Phys. Rev. Lett. **97**, 062001 (2006).
[40] S.-s. Fang, Int. J. Mod. Phys. A **21**, 839 (2006).
[41] Subhasis Basak *et al.*, Phys. Rev. D **76**, 074504 (2007).
[42] C. B. Lang, Prog. Part. Nucl. Phys. **61**, 35 (2008).
[43] S. H. Lee and H.-c. Kim, Nucl. Phys. **A612**, 418 (1997).
[44] D. Jido, M. Oka, and A. Hosaka, Phys. Rev. Lett. **80**, 448 (1998).
[45] Shi-Lin Zhu, W.-Y. P. Hwang, and Yuan-Ben Dai, Phys. Rev. C **59**, 442 (1999).
[46] F. X. Lee, Nucl. Phys. **A791**, 352 (2007).
[47] Frank X. Lee and Xinyu Liu, Phys. Rev. D **66**, 014014 (2002).
[48] L. A. Copley, G. Karl, and E. Obryk, Nucl. Phys. **B13**, 303 (1969).
[49] R. P. Feynman, M. Kislinger, and F. Ravndal, Phys. Rev. D **3**, 2706 (1971).
[50] R. Koniuk and N. Isgur, Phys. Rev. D **21**, 1868 (1980).
[51] S. Capstick, Phys. Rev. D **46**, 2864 (1992).
[52] S. Capstick and W. Roberts, Prog. Part. Nucl. Phys. **45**, S241 (2000).
[53] A. Manohar and H. Georgi, Nucl. Phys. **B234**, 189 (1984).
[54] Zhenping Li, Hongxing Ye, and Minghui Lu, Phys. Rev. C **56**, 1099 (1997).
[55] Z.-p. Li and B. Saghai, Nucl. Phys. **A644**, 345 (1998).
[56] J. He, X.-h. Zhong, B. Saghai, and Q. Zhao, arXiv:nucl-th/0710.4212 (2007).
[57] G. F. Chew, M. L. Goldberger, F. E. Low, and Y. Nambu, Phys. Rev. **106**, 1345 (1957).
[58] R. G. Moorhouse, Phys. Rev. Lett. **16**, 772 (1966).
[59] N. Isgur and G. Karl, Phys. Lett. **B74**, 353 (1978).
[60] N. Isgur and G. Karl, Phys. Rev. D **18**, 4187 (1978).
[61] N. Isgur and G. Karl, Phys. Rev. D **19**, 2653 (1979).
[62] N. Isgur and G. Karl, Phys. Lett. **B72**, 109 (1977).
[63] W.-M. Yao *et al.*, J. Phys. G **33**, 1 (2006).
[64] B. Krusche *et al.*, Phys. Rev. Lett. **74**, 3736 (1995).
[65] A. Bock *et al.*, Phys. Rev. Lett. **81**, 534 (1998).
[66] L. Tiator, C. Bennhold, and S. S. Kamalov, Nucl. Phys. **A580**, 455 (1994).
[67] M. Kirchbach and L. Tiator, Nucl. Phys. **A604**, 385 (1996).
[68] S.-L. Zhu, Phys. Rev. C **61**, 065205 (2000).
[69] V. G. J. Stoks and T. A. Rijken, Phys. Rev. C **59**, 3009 (1999).
[70] T. W. Morrison, Ph.D. thesis, George Washington University (1999).
[71] H. R. Crouch *et al.*, Phys. Rev. D **21**, 3023 (1980).
[72] F. Bulos *et al.*, Phys. Rev. Lett. **13**, 486 (1964).
[73] S. Capstick and W. Roberts, Phys. Rev. D **49**, 4570 (1994).
[74] B. S. Zou, Nucl. Phys. **A790**, 110c (2007).
[75] V. Kuznetsov and M. V. Polyakov, JETP Lett. **88**, 347 (2008).
[76] R. E. Cutkosky, C. P. Forsyth, R. E. Hendrick, and R. L. Kelly, Phys. Rev. D **20**, 2839 (1979).
[77] T. Mart and C. Bennhold, Phys. Rev. C **61**, 012201(R) (1999).
[78] K. Nakayama, Y. Oh, and H. Haberzettl, arXiv:0803.3169.
[79] V. Shklyar, G. Penner, and U. Mosel, Eur. Phys. J. A **21**, 445 (2004).
[80] R. Shyam and O. Scholten, arXiv:0808.0632.
[81] J. Durand, B. Julia-Diaz, Jun He, H. Lee, and B. Saghai (in preparation).
[82] Jun He, B. Saghai, and Zhenping Li (in preparation).
[83] V. Crede *et al.*, AIP Conf. Proc **915**, 729 (2007).